Steady three-dimensional convection at high Prandtl numbers

By H. FRICK†, F. H. BUSSE and R. M. CLEVER

Department of Earth and Space Sciences and Institute of Geophysics,
University of California, Los Angeles

Three-dimensional solutions are computed describing convection in a layer of a Boussinesq fluid of infinite Prandtl number. Rigid boundaries of constant temperature are assumed. As many as four physically different solutions are found for a given rectangular horizontal periodicity interval. These are two solutions describing bimodal convection, and two 'square-pattern' solutions which correspond to two orthogonally superimposed convection rolls of nearly equal amplitude. The Galerkin method used in obtaining the steady solutions can also be employed for the investigation of their stability. The stability of the bimodal solutions agrees with the experimental determination of the stability region by Whitehead & Chan (1976). The square-pattern solution is unstable in the investigated parameter range, even though it exhibits the highest Nusselt number.

1. Introduction

Convection in a layer heated from below represents the simplest fluid system that exhibits a sequence of transitions leading from two-dimensional laminar to more complicated three-dimensional and finally to turbulent states of motion. The relatively simple behaviour is primarily a reflection of the horizontal isotropy of the fluid layer. It is most strikingly apparent in high-Prandtl-number fluids in which the advection of heat is the dominant nonlinear process and the advection of momentum is negligible. The transition from two-dimensional to three-dimensional states of motion in high-Prandtl-number convection was investigated theoretically by Busse (1967). This work indicated that beyond the point of transition a bimodal-form convection is realized consisting of a basic roll motion and a superimposed roll motion of smaller wavelength and smaller amplitude. The work of Busse (1967) relied on a linear stability analysis of the basic two-dimensional rolls in order to infer properties of the three-dimensional state. The goal of this paper is to extend this analysis by investigating the fully nonlinear problem of three-dimensional convection.

For reasons of computational convenience much of the research on high-Rayleigh-number convection has focused on two-dimensional solutions. While convection rolls represent the physically realized form of convection up to a maximum of about fifteen times the critical value R_c of the Rayleigh number R in the case of rigid boundaries, only three-dimensional forms of convection are found at higher Rayleigh numbers. The use of two-dimensional solutions for the investigation of physical properties such as the heat transport is thus questionable at high Rayleigh numbers. Experimental observations do indeed indicate a strong increase of the heat transport beyond the transition to bimodal convection (Krishnamurti 1970). Other properties are also

† Present address: Kraftwerk Union, 605 Offenbach, W. Germany.

affected by the transition to the three-dimensional convection, and qualitatively new features may appear in connection with the new dimension of the flow, such as the vertical component of vorticity in finite-Prandtl-number fluids. Obviously, a much larger parameter space is available for three-dimensional forms of convection, and special choices must be made in the study of this parameter space. But even when the horizontal periodicity interval, described by two wavenumbers α_1 and α_2, is fixed, solutions of quite distinct form exist, as shown in this paper. Different solutions exhibiting the same symmetry and the same periodicity have not been found in the two-dimensional case, and were not expected when the computations reported in this paper were started.

In order to distinguish between different solutions a stability analysis is required. Only those solutions are physically realizable which are stable with respect to arbitrary three-dimensional disturbances. The stability analysis presented in this paper does not include the most general disturbances; but it appears to capture all physically relevant mechanisms of instability in a high-Prandtl-number fluid and yields good agreement with experimental observations. A remarkable finding is that the form of convection exhibiting the highest heat transport is unstable. The property of maximum heat transport thus does not seem to correlate well with the property of stability.

The paper starts with the mathematical formulation of the problem in §2. Bimodal solutions are described in §3 and their stability is studied in §4. Square-pattern convection and its stability properties are considered in §5. Some more general questions are addressed in the conclusion of the paper (§6).

2. Mathematical formulation of the problem

2.1. *Basic equations*

We consider a fluid layer of vertical thickness d and of infinite extent in the horizontal dimensions. The temperatures T_2 and T_1 are prescribed at the lower and upper boundaries respectively. Using the Boussinesq approximation we obtain dimensionless equations for the velocity vector $\mathbf{v}$ and for the deviation θ of the temperature distribution from the static state in the following form:

$$\nabla^2\mathbf{v} + \lambda\theta - \nabla\pi = P^{-1}\left(\mathbf{v}.\nabla\mathbf{v} + \frac{\partial\mathbf{v}}{\partial t}\right), \tag{2.1a}$$

$$\nabla.\mathbf{v} = 0, \tag{2.1b}$$

$$\nabla^2\theta + R\lambda.\mathbf{v} = \mathbf{v}.\nabla\theta + \frac{\partial\theta}{\partial t}. \tag{2.1c}$$

The physical parameters d, d^2/κ and $(T_2 - T_1)/R$ have been used as scales for length, time and temperature respectively, where κ is the thermal diffusivity. The unit vector λ is directed opposite to the gravity vector $\mathbf{g}$, and Rayleigh and Prandtl numbers are defined by

$$R = \frac{\gamma g(T_2 - T_1)\,d^3}{\nu\kappa}, \quad P = \frac{\nu}{\kappa}, \tag{2.2}$$

where γ is the coefficient of thermal expansion and ν is the kinematic viscosity. Equation (2.1b) and the dynamic pressure π can be eliminated from the problem by the introduction of the general representation of a solenoidal vector field

$$v = \nabla \times (\nabla \times \lambda\phi) + \nabla \times \lambda\psi \equiv \delta\phi + \varepsilon\psi. \tag{2.3}$$

Assuming the limit of infinite Prandtl number P, we find by taking the vertical component of the curl of (2.1a) that

$$\nabla^2 \Delta_2 \psi = 0. \tag{2.4}$$

In Cartesian coordinates with the z-coordinate in the direction of λ, the operator Δ_2 is defined by $\Delta_2 \equiv \partial^2/\partial x^2 + \partial^2/\partial y^2$. Since $\Delta_2 \psi$ must vanish at the rigid boundaries, (2.4) requires $\Delta_2 \psi \equiv 0$. This result implies $\varepsilon \psi \equiv 0$ because $\mathbf{v}$ is supposed to be bounded at infinity. The problem of convection in a fluid of infinite Prandtl number is thus reduced to two dependent variables, ϕ and θ. By operating with $\lambda \cdot \nabla \times (\nabla \times)$ on (2.1a) and by rewriting (2.1c) we obtain two equations for ϕ and θ:

$$\nabla^4 \Delta_2 \phi - \Delta_2 \theta = 0, \tag{2.5a}$$

$$\nabla^2 \theta - R \Delta_2 \phi = \delta \phi \cdot \nabla \theta + \frac{\partial \theta}{\partial t}. \tag{2.5b}$$

The corresponding boundary conditions are

$$\phi = \frac{\partial \phi}{\partial z} = \theta = 0 \quad \text{at} \quad z = \pm \tfrac{1}{2}. \tag{2.6}$$

2.2. *The steady problem*

Three-dimensional steady solutions of the nonlinear problem (2.5), (2.6) can be obtained by expanding ϕ, θ in terms of systems of orthogonal functions:

$$\phi = \sum_{lnm} a_{lnm} \cos l\alpha_1 x \cos n\alpha_2 y \, g_m(z) \equiv \sum_{lnm} a_{lnm} \phi_{lnm}, \tag{2.7a}$$

$$\theta = \sum_{lnm} b_{lnm} \cos l\alpha_1 x \cos n\alpha_2 y \, f_m(z) \equiv \sum_{lnm} b_{lnm} \theta_{lnm}. \tag{2.7b}$$

The functions

$$g_\nu(z) = \begin{cases} \dfrac{\sinh(\beta_{\frac{1}{2}\nu} z)}{\sinh(\frac{1}{2}\beta_{\frac{1}{2}\nu})} - \dfrac{\sin(\beta_{\frac{1}{2}\nu} z)}{\sin(\frac{1}{2}\beta_{\frac{1}{2}\nu})} & \text{for } \nu \text{ even} \\[4mm] \dfrac{\cosh(\lambda_{\frac{1}{2}(\nu+1)} z)}{\cosh(\frac{1}{2}\lambda_{\frac{1}{2}(\nu+1)})} - \dfrac{\cos(\lambda_{\frac{1}{2}(\nu+1)} z)}{\cos(\frac{1}{2}\lambda_{\frac{1}{2}(\nu+1)})} & \text{for } \nu \text{ odd} \end{cases} \tag{2.8a}$$

and

$$f_\nu(z) = \sin[\nu\pi(z + \tfrac{1}{2})] \tag{2.8b}$$

satisfy the boundary conditions for ϕ and θ respectively. The values β_ν and λ_ν are determined as the positive roots of

$$\coth \tfrac{1}{2}\beta - \cot \tfrac{1}{2}\beta = 0, \quad \tanh \tfrac{1}{2}\lambda + \tan \tfrac{1}{2}\lambda = 0$$

and are given in Chandrasekhar (1961, p. 636). The summations in (2.7) run through $0 \leqslant l, n < \infty$ and $1 \leqslant m < \infty$. After introducing the representation (2.7) into (2.5), multiplying (2.5a) by ϕ_{ijk} and (2.5b) by θ_{ijk}, and averaging the result over the fluid layer, a system of algebraic equations for the unknowns a_{lnm}, b_{lnm} is obtained;

$$L_{km}(i,j) a_{ijm} + b_{ijk} = 0, \tag{2.9a}$$

$$I_{km}(i,j) b_{ijm} + R J_{km}(i,j) a_{ijm} + N_{ijklnmpqr} a_{lnm} b_{pqr} = 0. \tag{2.9b}$$

The summation convention applies to any subscript occurring twice in any term. Since (2.9a) are linear, the unknowns a_{ijk} can be expressed in terms of b_{ijk} by a simple matrix inversion. The nonlinear system of equations (2.9b) can be solved by a

Newton–Raphson iteration method. In order to obtain a problem of finite dimension, the system of equations (2.9b) must be truncated. This is accomplished by neglecting unknowns b_{ijk} and equations with

$$i+j+k > N. \qquad (2.10)$$

By choosing sufficiently high values of N such that sensitive physical parameters, as for example the convective heat transport, do not change by more than a few per cent when N is replaced by $N-2$ it is expected that close approximation to the exact solution of (2.5) can be obtained. The total number of equations is reduced by the fact that solutions of physical interest exhibit the symmetry

$$\phi\left(\frac{\pi}{\alpha_1}-x, \frac{\pi}{\alpha_2}-y, -z\right) = -\phi(x,y,z), \qquad (2.11)$$

with an analogous relationship for θ. This symmetry translates into the property that there exists a subset of solutions of (2.9) for which unknowns a_{ijk}, b_{ijk} with odd $i+j+k$ vanish. This subset of solutions includes rolls, bimodal convection, square-pattern convection and related solutions. But there are other solutions which cannot be described by the subset. For instance, the case of a layer of convection rolls confined to the lower half of the fluid layer, $-\frac{1}{2} \leqslant z \leqslant 0$, superimposed by a mirror-symmetric second layer of convection rolls is not included in this subset, unless π/α_1 or π/α_2 is chosen as periodicity interval instead of $2\pi/\alpha_1$ or $2\pi/\alpha_2$. There is no indication that the solutions other than those included in the subset $i+j+k =$ even are physically observable.

The physical quantity of primary interest is the heat transport by convection. It can conveniently be described by the Nusselt number, which is the total heat transport divided by the heat transport in the case of the static solution,

$$Nu \equiv 1 - R^{-1}\frac{\partial\bar{\theta}}{\partial z}\bigg|_{z=\frac{1}{2}} = +R^{-1}\sum_m b_{00m} m\pi(-1)^{1+\frac{1}{2}m}. \qquad (2.12)$$

The bar indicates the horizontal average and the summation runs through all even integers m. The Nusselt number will be used in the following to characterize different sets of steady solutions.

2.3. *The stability problem*

In order to distinguish those steady solutions that are physically realizable a stability analysis must be performed. By superimposing arbitrary infinitesimal three-dimensional disturbances onto the steady solutions the following equations for the disturbance fields $\tilde{\phi}$ and $\tilde{\theta}$ are obtained:

$$\nabla^4\Delta_2\tilde{\phi} - \Delta_2\tilde{\theta} = 0, \qquad (2.13)$$

$$\nabla^2\tilde{\theta} - R\Delta_2\tilde{\phi} = \delta\tilde{\phi}.\nabla\theta + \delta\phi.\nabla\tilde{\theta} + \frac{\partial}{\partial t}\tilde{\theta}.$$

In this paper a restricted class of disturbances will be considered which can be represented in the form

$$\tilde{\phi} = \sum_{lmn} \cos l\alpha_1 x(\tilde{a}_{lnm}\cos n\alpha_2 y + i\breve{a}_{lnm}\sin n\alpha_2 y)g_m(z)\exp\{idy+\sigma t\}, \qquad (2.14a)$$

$$\tilde{\theta} = \sum_{lmn} \cos l\alpha_1 x(\tilde{b}_{lmn}\cos n\alpha_2 y + i\breve{b}_{lmn}\sin n\alpha_2 y)f_m(z)\exp\{idy+\sigma t\}. \qquad (2.14b)$$

The most general form of disturbances requires a replacement of $\cos l_{\alpha 1} x$ by

$$(\cos l\alpha_1 x + \hat{a}_{lnm} \sin l\alpha_1 x) \exp \{ibx\}$$

in (2.14) according to Floquet's theory. But since all observed instabilities can be described by disturbances (2.14) and since the x- and y-dependences of the steady solutions can be exchanged it does not seem necessary to do the much more expensive computations based on the most general form of disturbances.

As in the case of the steady solution a system of algebraic equations for the coefficients $\tilde{a}_{lnm}$, $\check{a}_{lnm}$, $\tilde{b}_{lnm}$, $\check{b}_{lnm}$ can be obtained from (2.13):

$$\tilde{L}_{km}(i,j)\,\tilde{a}_{ijm} + \hat{L}_{km}(i,j)\,\check{a}_{ijm} + \tilde{b}_{ijk} = 0, \tag{2.15a}$$

$$\tilde{L}_{km}(i,j)\,\check{a}_{ijm} - \hat{L}_{km}(i,j)\,\tilde{a}_{ijm} + \check{b}_{ijk} = 0, \tag{2.15b}$$

$$\tilde{I}_{km}(i,j)\,\tilde{b}_{ijm} + \hat{I}_{km}(i,j)\,\check{b}_{ijm} + R\{\tilde{J}_{km}(i,j)\,\tilde{a}_{ijm} + \hat{J}_{km}(i,j)\,\check{a}_{ijm}\}$$
$$+ \tilde{N}^{(1)}_{ijklmnpqr}\,\tilde{a}_{lmn}\,b_{pqr} + \tilde{N}^{(2)}_{ijklmnpqr}\,a_{lmn}\,\tilde{b}_{pqr} + \hat{N}^{(1)}_{ijklmnpqr}\,\hat{a}_{lmn}b_{pqr}$$
$$+ \hat{N}^{(2)}_{ijklmnpqr}a_{lmn}\check{b}_{pqr} + \sigma\tilde{b}_{ijk} = 0, \tag{2.16a}$$

$$\tilde{I}_{km}(i,j)\,\check{b}_{ijm} - \hat{I}_{km}(i,j)\,\tilde{b}_{ijm} + R\{\tilde{J}_{km}(i,j)\,\check{a}_{ijm} - \hat{J}_{km}(i,j)\,\tilde{a}_{ijm}\}$$
$$+ \tilde{N}^{(3)}_{ijklmnpqr}\,\check{a}_{lmn}b_{pqr} + \tilde{N}^{(4)}_{ijklmnpqr}\,a_{lmn}\check{b}_{pqr}$$
$$- \hat{N}^{(1)}_{ijklmnpqr}\,\tilde{a}_{lmn}b_{pqr} - \hat{N}^{(2)}_{ijklmnpqr}a_{lmn}\tilde{b}_{pqr} + \sigma\check{b}_{ijk} = 0. \tag{2.16b}$$

The coefficients $\tilde{a}_{ijk}$ and $\check{a}_{ijk}$ can be expressed in terms of the coefficients $\tilde{b}_{ijk}$ and $\check{b}_{ijk}$ by solving the linear system of equations (2.15). Equations (2.16a, b) then become a linear homogeneous system of equations with σ as eigenvalue. For a given steady solution and a given value of the parameter d the eigenvalue σ can be determined if the truncation (2.10) is used. Only the eigenvalue with maximum real part is of interest. When there exists as a function of d an eigenvalue σ with positive real part, the steady solution is unstable. If this is not the case, we shall regard the steady solution as stable.

3. Bimodal convection

Bimodal convection is described by a manifold of solutions bifurcating from solutions in the form of two-dimensional rolls. The name bimodal convection indicates that a second roll oriented at right angles to the basic roll pattern starts to grow at the point of transition. Because of the high amplitude of the basic roll solution the amplitude of the secondary roll remains relatively small in the range of Rayleigh numbers considered in this paper. Physically realized cases of bimodal convection are usually characterized by a higher wavenumber α_2 of the secondary roll; but bimodal solutions of (2.9) exist even for $\alpha_2 < \alpha_1$. The property of secondary bifurcation is thus the fundamental feature of bimodal convection. It distinguishes it from square-pattern convection, which bifurcates from the static state just as roll solutions do. In table 1 Nusselt numbers for typical examples of bimodal convection and square-pattern convection are listed for comparison. Although the term square-pattern convection was used originally for solutions with $\alpha_1 = \alpha_2$ that are invariant with respect to an interchange of the x- and y-dependences, in this paper solutions with $\alpha_1 \neq \alpha_2$ are referred to as square-pattern convection as long as they evolve continuously from the case $\alpha_1 = \alpha_2$. In contrast to bimodal convection they are characterized by rather similar values for the coefficients b_{l0m} and b_{0lm}. Throughout this section the dominant basic-roll part of the bimodal solution is assumed to be

R	N	Bimodal convection, $\alpha_1 = 3.117$			Square convection, $\alpha_1 = 3.117$		2-dimensional convection $\alpha_1 = 3.117$
		$\alpha_2 = 4.0$	$\alpha_2 = 5.0$	$\alpha_2 = 6.0$	$\alpha_2 = 3.117$	$\alpha_2 = 410$	
30×10^3	8	3.506	3.652	3.502	3.702	3.809	—
	10	3.452	3.587	3.454	3.637	3.735	3.427
	12	3.434	3.563	3.438	3.610	3.704	3.410
35×10^3	8	3.670	3.896	3.821	3.860	3.983	—
	10	3.597	3.813	3.747	3.783	3.896	—
	12	3.574	3.778	3.717	3.751	3.858	3.532
40×10^3	8	3.818	4.106	4.074	4.002	4.138	—
	10	3.726	4.010	3.984	3.914	4.040	—
	12	3.698	3.966	3.943	3.876	3.995	3.640
45×10^3	8	3.952	4.289	4.282	4.131	4.278	—
	10	3.842	4.188	4.184	4.033	4.171	—
	12	3.887	4.135	4.132	3.989	4.119	—
50×10^3	10	3.949	4.355	4.356	4.142	4.292	—
	12	3.909	4.293	4.294	4.093	4.233	3.827
60×10^3	10	4.142	—	4.644	—	4.509	—
	12	—	—	4.567	—	—	—
70×10^3	10	4.315	—	—	—	—	—
	12	4.248	—	—	—	—	4.131

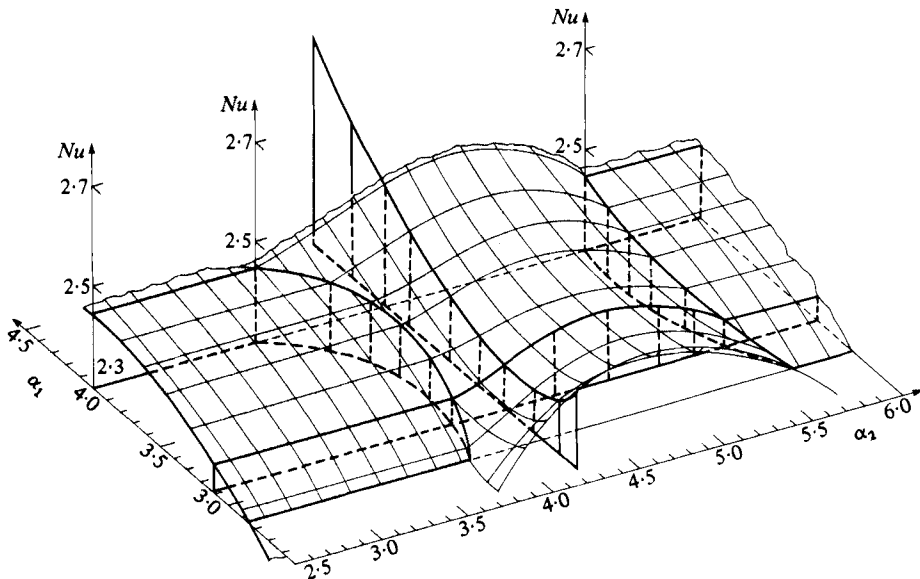TABLE 1. Nusselt number as a function of the Rayleigh number R for typical examples of convection solutions

FIGURE 1. The Nusselt number at $R = 26 \times 10^3$ as a function of α_1, α_2, for bimodal convection and y-independent rolls. The bimodal solutions bifurcate from the latter solution in the (Nu, α_1, α_2) space at curves determined by the stability analysis of Busse (1967). Thick lines represent computed values, thin lines estimated values.

Table 2. Nusselt number for bimodal convection as a function of α_1, α_2 at selected Rayleigh numbers (truncation parameter $N = 8$)

$\alpha_1 = 3\cdot117$, α_2 given below

R	3·8	3·9	4·0	4·1	4·2	4·3	4·5	4·7	4·9	5·1	5·2	5·3
23×10^3	—	—	—	—	3·255	3·262	3·296	3·265	—	—	—	—
24×10^3	—	3·285	—	3·290	3·301	3·310	3·322	3·323	3·311	3·286	—	3·285
26×10^3	3·351	3·351	3·359	3·374	3·389	3·402	3·423	3·434	3·432	3·417	3·404	—

$\alpha_2 = 4\cdot0$, α_1 given below

R	2·5	2·9	3·117	3·5	4·0	4·25	$\alpha_1 = 3\cdot117$, $\alpha_2 = 5\cdot0$
30×10^3	3·556	3·494	3·506	3·552	3·660	3·730	3·652

$\alpha_2 = 4\cdot2$, α_1 given below

R	2·6	2·7	2·9	3·117	3·3	4·2	4·5
26×10^3	3·449	2·415	3·388	3·389	3·403	3·591	3·690

Table 3. Nusselt number of square-pattern convection as a function of α_1, α_2 at two Rayleigh numbers (truncation parameter $N = 8$)

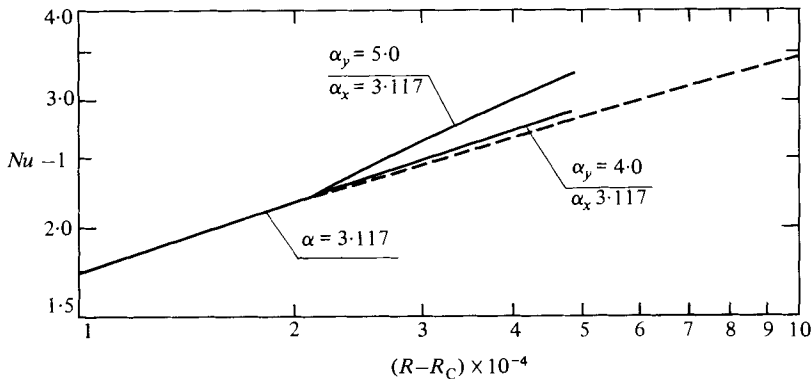| R	$\alpha_1 = 2\cdot5$, $\alpha_2 = 2\cdot5$	$\alpha_1 = 3\cdot117$, $\alpha_2 = 3\cdot117$	$\alpha_1 = 2\cdot9$, $\alpha_2 = 3\cdot117$	$\alpha_1 = 4\cdot2$, $\alpha_2 = 4\cdot2$	$\alpha_1 = 3\cdot117$, $\alpha_2 = 3\cdot3$	$\alpha_1 = 3\cdot117$, $\alpha_2 = 4\cdot0$	$\alpha_1 = 3\cdot3$, $\alpha_2 = 4\cdot2$	$\alpha_1 = 3\cdot8$, $\alpha_2 = 4\cdot2$
26×10^3	3·344	3·560	3·524	3·766	3·586	3·702	3·694	3·743
30×10^3	—	3·809	—	—	—	—	—	—

FIGURE 2. The Nusselt number as function of the Rayleigh number for
roll $(\alpha_1 = 3\cdot117)$ and two bimodal solutions.

associated with the wavenumber α_1. There exist, of course, a corresponding class of
bimodal solutions for which x- and y-dependences are interchanged.

The Nusselt number of bimodal convection as a function of α_1, α_2 is shown in figure
1. Only the thick lines in that figure connect actually calculated values; but the
Nusselt-number surface is sufficiently smooth that an extrapolation from the
computed values seems justified. Most of the computed values used in the figure have
been listed in table 2. The values $\alpha_2 = \alpha_2^*$ at which the bimodal solution reduces to
the two-dimensional roll solution have been obtained from the stability analysis of
Busse (1967). The values α_2^* represent the cases for which the growth rates of
disturbances of two-dimensional rolls vanish. Numerical results not published in
Busse (1967) have been used for the determination of α_2^*.

As expected, bimodal convection exhibits a heat transport exceeding that of the
corresponding two-dimensional solution. Depending on the kind of bimodal
convection realized the change of slope in the heat-transport curve at the transition
to bimodal convection is more or less pronounced as shown in figure 2. The reason
for the increased heat transport is not clearly evident from the form of the solution.
Lines of constant vertical velocity in the midplane of the layer, streamlines and
isotherms are shown in figure 3. It had been expected that the streamlines of the
short-wavelength roll component of bimodal convection would penetrate strongly
into the thermal boundary layers of $z = \pm\frac{1}{2}$. Only a rather weak effect of this nature
is evident in the figure.

The large number of parameters and the expense of computing prohibit a much
more detailed investigation of the manifold of solutions describing bimodal convec-
tion. Most computations have been done with $N = 8$, which yields Nusselt numbers
within 2 or 3 % of the exact value for $R \leqslant 3 \times 10^4$ if results obtained for $N = 10$ are
used as a guide. For higher Rayleigh numbers truncation parameters $N = 10$ and 12
have been used as shown in table 1. Because of the more rapidly increasing number
of higher harmonics with N, three-dimensional solutions appear to converge much
faster than two-dimensional solutions at the same value of N. Problems of convergence
have restricted the number of computations of steady bimodal convection in some
cases. It has not been possible, for example, to extend the wavenumber α_2 in the case
$R = 26 \times 10^3$, $\alpha_1 = 4\cdot2$ beyond the interval $2\cdot6 \lesssim \alpha_2 \lesssim 4\cdot5$. At both ends of this
interval the Nusselt number tends to increase sharply and the coefficients b_{0nm} grow
rapidly in comparison with the coefficients b_{nom}. This suggests that the surface of
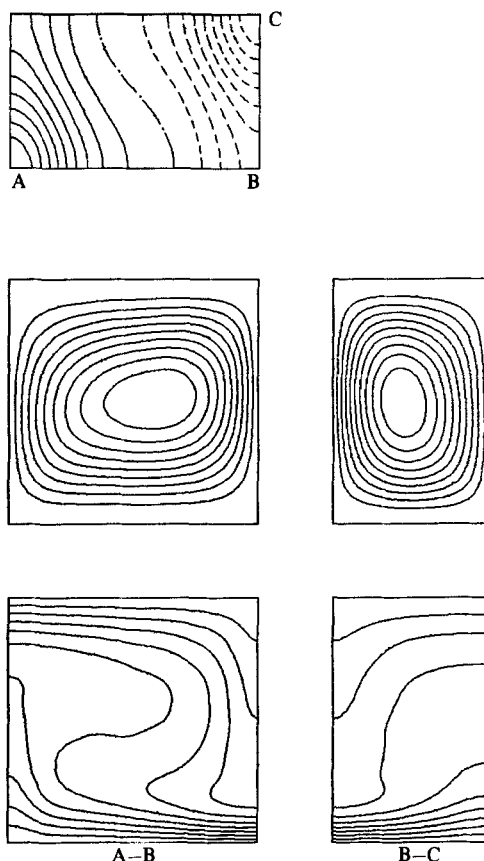
FIGURE 3. Lines of constant vertical velocity v_z in the plane $z = 0$ (negative values are dashed) are shown in upper left graph. Lines of constant $\partial_x \phi$ in the plane $y = 0$ (A–B) and lines of constant $\partial_y \phi$ in the plane $x = \pi/\alpha_1$ (B–C) are shown in the two middle graphs. The corresponding isotherms are shown in the two lower graphs.

bimodal solution in the (Nu, α_1, α_2) parameter space may bend over to join the upper surface of square-pattern convection which is discussed in §5. A different numerical scheme will be required to verify this hypothesis.

4. Stability of bimodal convection

All two-dimensional solutions shown in figure 1 are unstable since there always exists a disturbance of bimodal nature which is growing when the Rayleigh number exceeds 22 600 according to the stability theory of Busse (1967). But the bimodal solutions are not always stable either. The stability of bimodal convection has been investigated experimentally in a high-Prandtl-number fluid by Whitehead & Chan (1976). When the wavenumber α_2 was controlled by appropriate initial conditions at the onset of transition to bimodal convection, these authors found that sometimes an instability occurred which replaced the bimodal pattern by a pattern with a different α_2 while the wavenumber α_1 of the basic rolls remained unchanged.

Motivated by the experimental study, the stability of bimodal solutions with respect to disturbances of the form (2.14) has been investigated. A typical stability
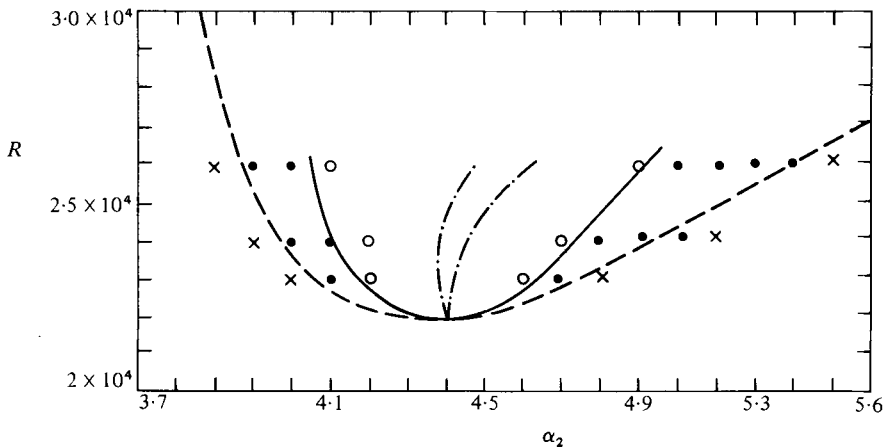
FIGURE 4. Stability of bimodal solutions with $\alpha_1 = 3 \cdot 117$ as a function of R and α_2. Stable solutions (O) are founded by the solid curve. Solutions indicated by a dot ($\cdot$) are unstable with respect to disturbances introducing wavenumbers α_2 within the dot–dashed lines. Points at which a bimodal solution could not be obtained are denoted by ($\times$). No bimodal solutions have been found outside the dashed curve determined from the stability computations of Busse (1967). (The single exception at $R = 24 \times 10^3$ lies outside the dashed curve at a distance which is within the uncertainity of the different numerical schemes.)

region is shown in figure 4. The outer parabolically shaped curve encloses the region of steady bimodal solutions. The curve representing values α_2^* as a function of the Rayleigh number has been derived from unpublished results of the analysis described by Busse (1967). The inner parabolically shaped curve encloses the region of stable steady bimodal solutions. Growing disturbances outside the latter curve are characterized by finite values of d, which indicates the tendency of the disturbances to change the wavenumber α_2. Indeed the values of $\alpha_2 + d$ in the case of the left region of instability and $\alpha_2 - d$ in the case of the region of instability on the right side fall within the dash-dotted lines at the centre of the stability region. The instability is thus analogous to the Eckhaus instability which limits the region of stable rolls near the critical Rayleigh number for onset of convection.

A comparison with the stability diagram determined by Whitehead & Chan for the case $\alpha_1 = 2 \cdot 5$ in a convection layer with $P = 126$ shows a close resemblance. The width of the region of stable values α_2 is about the same, and the preferred wavenumber α_2 that is attained as a result of instabilities shows an increase with increasing Rayleigh number. Because of the finite conductivity of the boundaries used in the experiment, the observed wavenumbers tend to be smaller than those predicted by the theory based on infinitely conducting boundaries. This effect is caused by the increased region in the z-direction over which temperature fluctuations exist with significant amplitude. It can thus be expected that quantitative agreement will be obtained if theory and experiment use identical boundary conditions. Since the experiments did not indicate any other mechanism of instability, it does not seem worthwhile to embark on a more complete analysis of the stability of bimodal convection than that described by the ansatz (2.14). While in principle this ansatz permits the analysis of the oscillatory instability of bimodal convection, such an instability has not been found, in agreement with the experiment observation that the Rayleigh number for the onset of this instability increases strongly with the Prandtl number (Busse & Whitehead 1974).
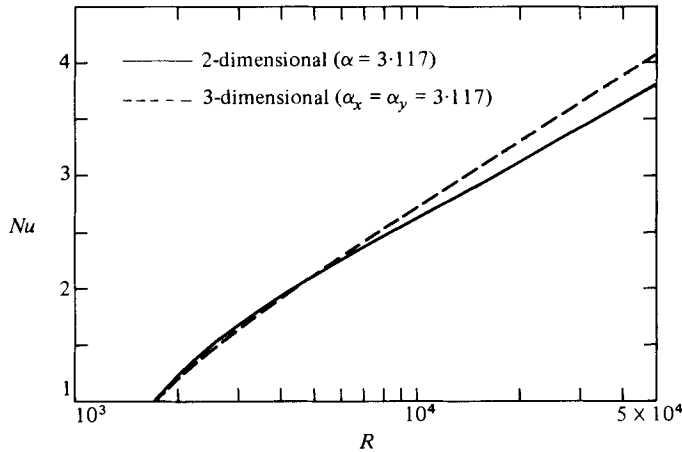
FIGURE 5. The Nusselt number for square-pattern convection ($\alpha_x = \alpha_y = 3{\cdot}117$, dashed) in comparison with the Nusselt number for rolls ($\alpha = 3{\cdot}117$).

5. Square-pattern convection

Square-pattern convection plays an enigmatic role in the science of convection. It has been predicted as a stable form of convection in the case of nearly insulating boundaries of the convection layer (Busse & Riahi 1980). Observations are not available for this limit. Instead square-pattern convection has been observed in cases of doubly diffusive convection (Shirtcliffe & Turner 1970) and in high-Prandtl-number convection with strongly temperature-dependent viscosity (Oliver 1980). In high-Prandtl-number experiments with constant viscosity there is some evidence that square-pattern convection becomes stable when the Rayleigh number exceeds 10^5 by a considerable margin (Whitehead & Parsons 1978). All these results are not in conflict with the findings of the present theoretical analysis, since all square-pattern solutions obtained here turned out to be unstable with respect to infinitesimal disturbances.

The instability of square-pattern solutions is surprising since their heat transport exceeds that of rolls and even that of most bimodal solutions, as is shown in figure 5. Near the critical Rayleigh number the heat transport by square-pattern convection is relatively low, in agreement with the small-amplitude analysis of Schlüter, Lortz & Busse (1965). But at Rayleigh numbers of order 5×10^3 it begins to exceed the heat transport by rolls and the asymptotic power law for the Nusselt–Rayleigh-number relationship appears to be distinctly different.

As pointed out earlier, the manifold of square-pattern solutions include solutions for which α_1 and α_2 are different as long as the corresponding solutions evolve smoothly from the special case $\alpha_1 = \alpha_2$. Since the x- and y-dependences can be interchanged, there are two surfaces of square-pattern solutions which intersect at the plane $\alpha_1 = \alpha_2$ in the (Nu, α_1, α_2) parameter space as shown in figure 6. Convergence problems in the use of the Newton–Raphson iteration scheme have prevented us from extending the surfaces much further, although not as determined an effort has been made as in the case of bimodal convection. Selected numerical values used in drawing figure 6 have been listed in table 3.

The stability analysis of square-pattern solutions is relatively simple since the most strongly growing disturbances appear to be characterized by $d = 0$. This indicates that the instability does not change the periodicities of the solution and that a bimodal form of convection or roll convection for $R \lesssim 22\,600$ is approached as the
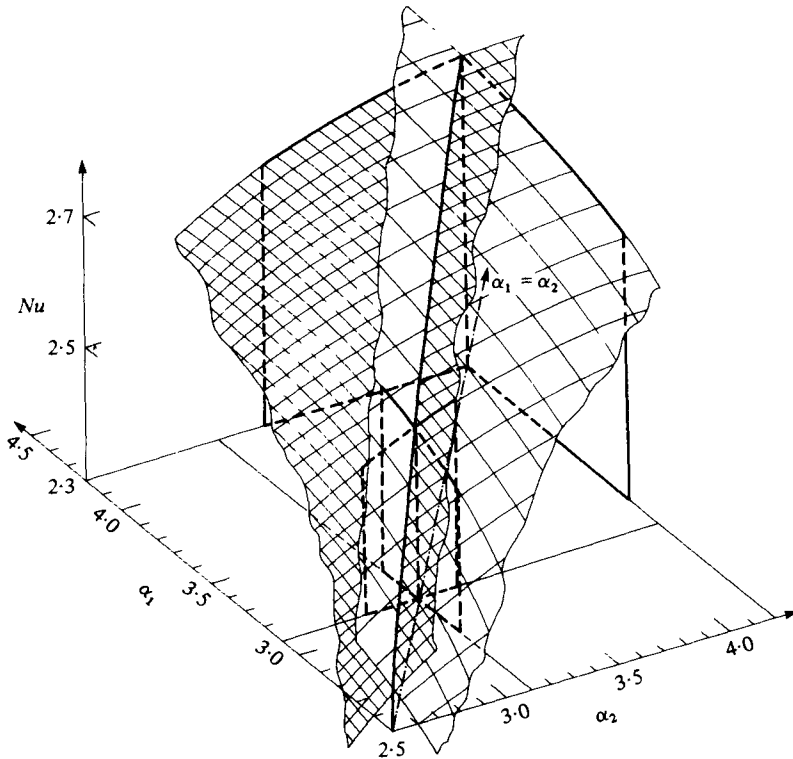
FIGURE 6. The two intersecting surfaces of Nusselt numbers for square-pattern convection at $R = 26 \times 10^3$. Only the thick lines have been computed.

disturbances grow to finite amplitude. The growth rates of disturbances are not very large and it seems likely that an additional physical effect or higher Rayleigh numbers than those achieved in the present computations could lead to a regime of stable square-pattern convection.

6. Concluding remarks

The most surprising result of the computations reported in this paper is the existence of three three-dimensional solutions describing convection in a square periodicity interval $\alpha_1 = \alpha_2$ and four such solutions for $\alpha_1 \neq \alpha_1$. In the case $\alpha_1 = \alpha_2$ the two bimodal solutions can be transformed into each other by interchanging the x- and y-dependences, while the square-pattern solution is symmetric in x and y. For $\alpha_1 \neq \alpha_2$ two square-pattern solutions evolve from the single solution of the case $\alpha_1 = \alpha_2$ as shown in figure 6. It is not unlikely that the surfaces of the two manifolds of bimodal solution become connected with the two manifolds of square-pattern solutions as $|\alpha_1 - \alpha_2|$ increases in the (Nu, α_1, α_2) space. The topological properties of hypersurfaces of manifolds of solutions in an appropriate parameter space have received little attention so far, and extensions of the solutions described in this paper could eventually provide an interesting example for the study of those hypersurfaces.

The bifurcation of bimodal solutions from the two-dimensional solution is similar in many respects to the bifurcation of the two-dimensional solution from the static

solution. In both cases new spatial degrees of freedom are occupied by the bifurcating solutions or, in other words, symmetries of horizontal translations are broken. As a consequence of this property the heat transport exhibits a kink at the point of transition and the range of the wavenumbers accessible beyond the lowest point of truncation grows quadratically with the excess of the Rayleigh number over the critical value. The sideband mechanism of instability restricts the α_2 region of stable bimodal solutions near the Rayleigh number of onset by the same factor $3^{-\frac{1}{2}}$ as in the case of the Eckhaus instability of two-dimensional rolls (Busse 1971). Instabilities involving three spatial dimensions occur differently in the case of rolls and bimodal convection. But similarities are still apparent as has been emphasized in the case of the oscillatory instability (Busse & Whitehead 1974).

The fact that square-pattern solutions are unstable with respect to disturbances growing at a relatively low rate suggests that appropriate changes in the physical parameters of the problem may lead to a physical realization of these solutions. Temperature dependence of the viscosity is a possibility suggested by experimental observations (Oliver 1980). Computations extending the present analysis to that case are presently under preparation. The properties determining the relative stability of rolls and square-pattern convection or of bimodal and square pattern convection are not obvious. The convective heat transport appears to have little influence on the relative stability, as the results of this paper have shown.

REFERENCES

BUSSE, F. H. 1967 On the stability of two-dimensional convection in a layer heated from below. *J. Fluid Mech.* **46**, 140–150.

BUSSE, F. H. 1971 Stability regions of cellular fluid flow. In *Instability of Continuous Systems* (ed. H. Leipholz), pp. 41–47. Springer.

BUSSE, F. H. & RIAHI, N. 1980 Nonlinear convection in a layer with nearly insulating boundaries. *J. Fluid Mech.* **96**, 243–256.

BUSSE, F. H. & WHITEHEAD, J. A. 1974 Oscillatory and collective instabilities in large Prandtl number convection. *J. Fluid Mech.* **66**, 67–79.

CHANDRASEKHAR, S. 1961 *Hydrodynamic and Hydromagnetic Stability*. Oxford University Press.

KRISHNAMURTI, R. 1970 On the transition to turbulent convection. Part 1. The transition from two- to three-dimensional flow. *J. Fluid Mech.* **42**, 295–307.

OLIVER, D. S. 1980 Bénard convection with strongly temperature-dependent viscosity. Ph.D. dissertation, University of Washington.

SCHLÜTER, A., LORTZ, D. & BUSSE, F. H. 1965 On the stability of steady finite amplitude convection. *J. Fluid Mech.* **23**, 129–144.

SHIRTCLIFFE, T. G. L. & TURNER, J. S. 1970 Observations of the cell structure of salt fingers. *J. Fluid Mech.* **41**, 707–719.

WHITEHEAD, J. A. & CHAN, G. L. 1976 Stability of Rayleigh–Bénard convection rolls and bimodal flow at moderate Prandtl number. *Dyn. Atmos. Oceans* **1**, 33–49.

WHITEHEAD, J. A. & PARSONS, B. 1978 Observations of convection at Rayleigh numbers up to 760000 in a fluid with large Prandtl number. *Geophys. Astrophys. Fluid Dyn.* **9**, 201–217.